SAND2023-03166C

Investigations of Farm-to-Farm Interactions and Blockage Effects from AWAKEN Using Large-Scale Numerical Simulations

Lawrence Cheung[1], Alan Hsieh[2], Myra Blaylock[1], Thomas Herges[2], Nathaniel deVelder[2], Kenneth Brown[2], Philip Sakievich[2], Daniel Houck[2], David Maniaci[2], Collen Kaul[3], Raj Rai[3], Nicholas Hamilton[4], Alex Rybchuk[4], Ryan Scott[4], Regis Thedin[4], Michael Brazell[4], Matthew Churchfield[4], Michael Sprague[4]

[1] Sandia National Laboratories, Livermore, CA 94550, USA
[2] Sandia National Laboratories, Albuquerque, NM 87185, USA
[3] Pacific Northwest National Laboratories, Richland WA 99354, USA
[4] National Renewable Energy Laboratory, Golden, CO 80401, USA

Corresponding author email: lcheung@sandia.gov

Abstract. A large-scale numerical computation of five wind farms was performed as a part of the American WAKE experimeNt (AWAKEN). This high-fidelity computation used the ExaWind/AMR-Wind LES solver to simulate a 100 km × 100 km domain containing 541 turbines under unstable atmospheric conditions matching previous measurements. The turbines were represented by Joukowski and OpenFAST coupled actuator disk models. Results of this qualitative comparison illustrate the interactions of wind farms with large-scale ABL structures in the flow, as well as the extent of downstream wake penetration in the flow and blockage effects around wind farms.

1. Introduction

The American WAKE experimeNt (AWAKEN) is a field campaign with the aim of producing detailed observations of atmospheric interactions with wind farms, in order to improve understanding of wind farm physics and overall performance. Centered around five wind farms in northern Oklahoma, the campaign began in September 2022 and will run through at least October 2023.

The AWAKEN campaign will synthesize measurement data with complementary simulations using a variety of tools of varying levels of fidelity. The suite of simulations includes some of the highest fidelity wind farm models run to date, some of which are presented herein, as well as lower fidelity engineering models. These simulations will validate the accuracy of models and provide improved understanding of wind farm flow physics. Researchers will use these simulations and observations to create a set of publicly available benchmarks that will be valuable for the international wind energy community.

The application of large-eddy simulation (LES) to wind plant/farm flows has been of interest to researchers for several years, of which two reviews on the topic were performed by Mehta et al. [1] and Breton et al. [2]. Recently, Centurelli et al. [3] found that analytical models consistently underestimate the upstream velocity deficit (i.e., blockage) on the farm scale. Using LES and two-scale momentum theory, Kirby et al. [4] developed a new method to quantify turbine-scale losses that

depends on the atmospheric response to the farm as a whole. As a part of AWAKEN, Sanchez-Gomez et al. [5] use weather research and forecasting (WRF) LES to assess farm-level blockage in the presence of terrain. Strickland led two papers in 2022 using LES to study wind farm blockage in both the stable [6] and neutral [7] atmospheric boundary layer (ABL). LES of wind farms are complemented by field observations of both blockage and wakes. Farm-level blockage is the focus of Bleeg et al. [8], in which they detail field observations at three wind farms. They suggest that the absence of farm level upstream blockage/induction effects can cause a significant overprediction when modeling farm performance. More recently, Schneemann et al. [9] measured the inflow to a 400 MW offshore farm with scanning long-range Doppler lidar, showing significant differences in farm-level blockage between stable and unstable stratifications.

Concerning wakes, Platis et al. [10] measured differences in wake development and persistence in varying atmospheric stratifications. The airborne measurement campaign of Cañadillas et al. [11] showed a nearly 35 km wake length difference between farms in stably and unstably stratified atmospheric conditions. Sebastiani et al. [12] used over 10 years of SCADA data from the Lillegrund wind farm to analyze performance and inform model development. They calculated a 28% power loss due to the clustering of turbines and traced an altered stability cycle offshore, given water's larger thermal capacity, as well as estimating a 2% loss due to farm-level blockage.

1.1. Objectives

The primary aim of this work is to simulate the entire five wind farm domain, as it is being instrumented and analyzed in the AWAKEN field campaign. The authors intend to address multiple stability conditions (unstably and stably stratified) but currently focus on unstable stratification. Large scale changes to the ABL as well as interactions with ABL structures due to presence of wind farms will be addressed. Ultimately, results of this work will support various science questions within the AWAKEN project and inform the experimental analysis. LES simulations of this scale can predict both farm-level blockage and address questions on multi-farm induction. When virtual instrumentation is implemented, simulations will also help determine what phenomena are measurable in planned lidar and radar data sets. This work will also support future comparisons to other tools (WRF, FLORIS [FLOw Redirection and Induction in Steady State], FAST.Farm), informing both engineering-level models and parameterizations in mesoscale atmospheric models.

2. Methodology

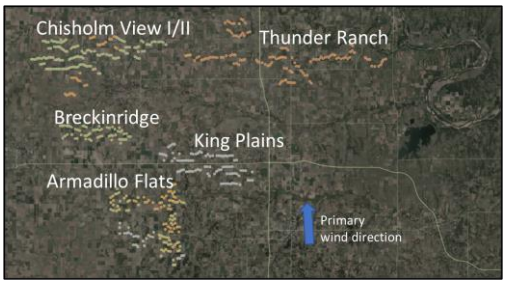

Figure 1 – Left: Schematic of the five wind farms studied as a part of AWAKEN in northern Oklahoma

Table 1. Overview of the AWAKEN wind farms

Farm	Capacity (MW)	Turbine types
King Plains	248.2	GE 2.8-127
Armadillo Flats	247.3	GE 1.79-100, GE 1.715-100, GE 2.3-116
Breckinridge	98.1	GE 1.7-103
Chisholm View I, Chisholm View II	235.2 64.8	GE 1.68-82.5, GE 2.4-107
Thunder Ranch	297.8	GE 2.5-116, GE 2.3-116
Total	**1,191.4**	**541 turbines**

2.1. AWAKEN overview and conditions

The design of the AWAKEN experiment is centred around observations and companion simulations relevant for science goals ranging from individual turbine wakes and turbulence within wind farms to larger scale wind farm wakes and the impacts of dynamic atmospheric events. The general layout of

the AWAKEN wind site is shown in Figure 1 and is comprised of five wind farms with a total of 541 turbines and an overall generating capacity of 1.19 GW (see Table 1). A variety of instruments will be placed at various locations and turbines within the site to measure winds, temperature, surface fluxes and other atmospheric quantities of interest. Of particular interest to the campaign is the phenomena occurring near the King Plains wind farm, and how it interacts with the surrounding wind farms wakes and atmospheric inflow. Most of the deployed instruments, including radar, turbine mounted lidars, and met mast stations, are located in and around the King Plains area, so simulations of this region would allow for direct comparison with experimental measurements. Additional details on the AWAKEN measurement campaign can be found in the overview of Moriarty et al. [13].

The conditions for the numerical simulations are derived from measurements at the nearby Atmospheric Radiation Measurement (ARM) Climate Research Facility. Table 2 shows the data taken at the Central C1 location of ARM, and includes wind speed, turbulence, and shear information collected over the period from Jan. 2015 to Nov. 2020. In all cases the primary wind direction was 175 ± 10 degrees. Data corresponding to both unstable and stable conditions was available, although the current study focuses on simulations of the unstable ABL, with results of the stable case appearing in future work.

Table 2. Measured wind conditions at the ARM C1 central location

Parameter	Unstable ABL	Stable ABL
Wind speed (z=91 m)	9.0 m/s	10.05 m/s
Wind shear exponent	0.0898	0.322
Potential temperature (z=3 m)	305.803 K	302.34 K
Friction velocity	0.486 m/s	0.323 m/s
Turbulence intensity (z=60 m)	18.04%	9.56%

2.2. Numerical methodology

In this work we use the ExaWind/AMR-Wind solver [14] to enable efficient and scalable simulations of wind power plants. Its block-structured refinements enable more efficient algorithms such as Multi-Level Multi-Grid (MLMG) and is well suited for next generation supercomputers with GPUs.

AMR-Wind solves the incompressible Navier-Stokes equations with variable density and viscosity. Additionally, scalar transport equations can be solved, such as potential temperature or turbulent kinetic energy. The discretization in AMR-Wind is based on the approximate projection method used in IAMR [15] and incflo [16]. It is a semistaggered scheme in which the velocity and scalar variables are located at cell centers and pressure is located at nodes. Pressure is also staggered in time so that pressure and the pressure gradient are recorded at time $n + 1/2$. The time discretization is handled with a Crank Nicolson approach, and the advection term is handled explicitly using an upwind finite-volume method using the WENO-Z algorithm. The diffusion terms can be handled explicitly, semi-implicitly, or implicitly and are spatially discretized using a second-order central difference formula. For the simulations in this paper, we use an implicit scheme for the viscous terms, as the variable viscosity from the eddy viscosity may cause time step restrictions. After the scalar equations and the momentum equations are advanced in time, a nodal projection is used to approximately correct the velocity field to make it divergence free.

In all simulations with AMR-Wind, both the Coriolis forcing and Boussinesq buoyancy model were included to capture the effects of wind veer and atmospheric stratification. The subgrid-scale kinetic energy one-equation turbulence model was employed to close the LES equations. At the lower boundary, the subgrid scale stresses are applied following the formulation of [17]. Based on an analysis of available radiosonde data, a temperature inversion was also applied at $z = 1500$ m to limit the growth of the ABL in the vertical direction. This was created by setting the potential temperature from 0 to 1400 m to 305.803 K, then linearly increasing to 313.803 K at 1500 m and 314.553 at 2560

m. These simulations do not account for terrain effects, and a flat lower surface with modeled surface roughness is used.

2.3. Precursor calculations

The wind farm simulations performed in this study were carried out in a two-stage process. In the first stage, a precursor calculation is used to develop the correct ABL inflow boundary conditions. The precursor calculation used an ABL forcing scheme where a constructed pressure gradient was applied to ensure that the hub-height wind speed at z=91 m matched the ARM measurements, and horizontally periodic boundary conditions were used. To arrive at the correct shear and turbulence intensity characteristics, two wall model parameters were varied at the ground: the surface roughness z_0 and the applied surface temperature flux at the ground. The values that produced the closest match to the observed turbulence intensity and wind shear are $z_0 = 0.15$ and a surface temperature flux of 0.0442

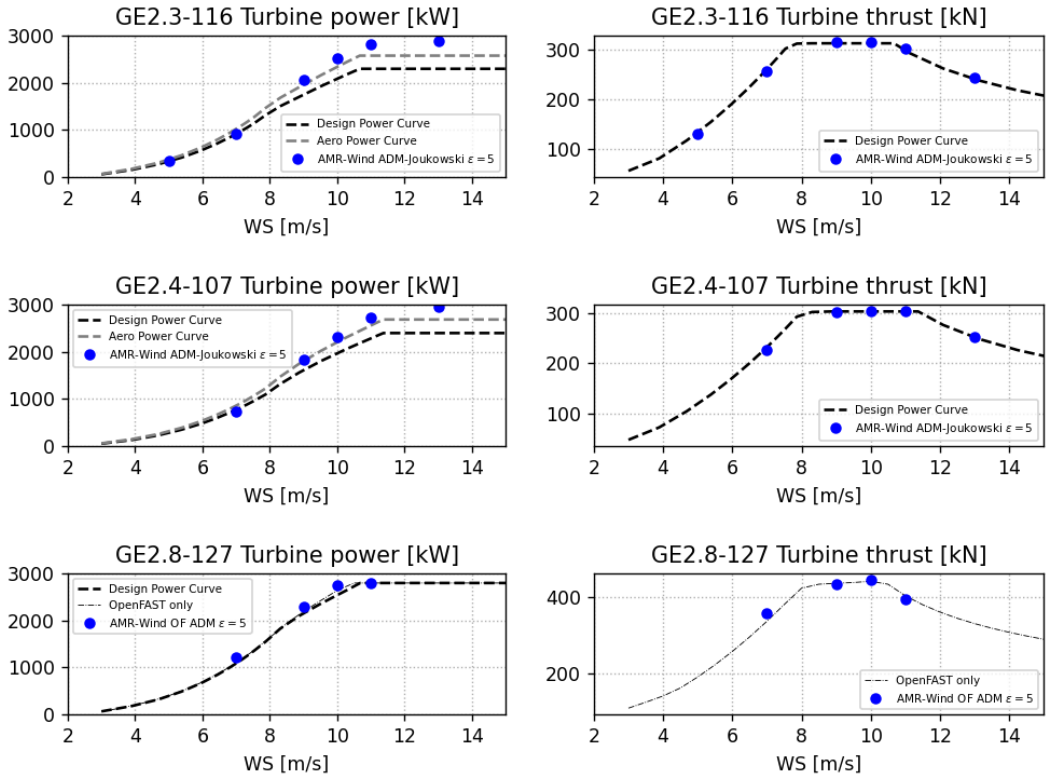

Figure 2 – Power and thrust curves for selected turbines used in the AWAKEN simulation.

K-m/s. Future simulations will also explore the use of inflow velocity and temperature forcing derived from idealized mesoscale WRF simulations.

Once the appropriate ABL conditions are established, the second stage of the simulation uses the precursor solution as the initial condition and the saved boundary data as the inflow conditions. These calculations include additional mesh refinement and turbine models to capture the full operation of the AWAKEN wind farms.

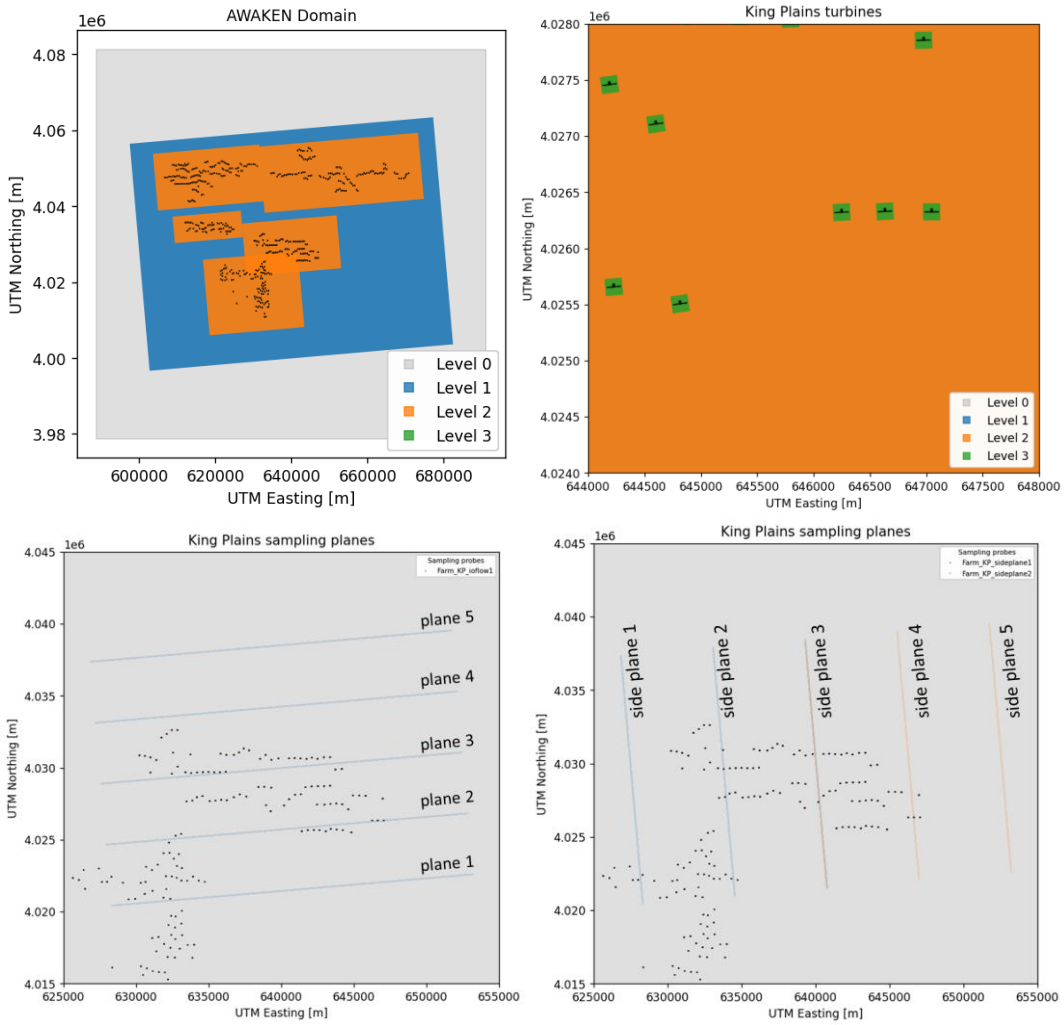

Figure 3 – Top row: Mesh layout and refinement zones for the full AWAKEN simulation domain. Bottom row: Inflow/outflow and streamwise side sampling planes used for the King Plains wind farm.

2.4. Turbine representation

The turbines in each wind farm are modeled using source term representations of the rotor in AMR-Wind, specifically two different versions of the actuator disk model (ADM). For the 88 turbines at the King Plains wind farm, the actuator disk model in AMR-Wind is coupled with OpenFAST. To compute turbine loading, fluid properties are first sampled at discrete ADM points, which are spaced at equidistant locations across the entire swept area of the rotor. Actuator forces use OpenFAST's suite of engineering models to characterize the wind turbine dynamics including the blade aerodynamics, control system, and structural loading. The actuator body-forces are then distributed back to the fluid domain in AMR-Wind using an isotropic smoothing kernel, and the average forces for the blades are spread azimuthally between the discrete ADM sampling points.

For the turbines at the Armadillo Flats, Chisholm View, Thunder Ranch, and Breckinridge wind farms, a simpler actuator disk model was used. The constant circulation model described in [18], corresponding to a Joukowski actuator disk, was implemented in AMR-Wind and used for those turbines. In this model, only the rotor speed and thrust coefficient curves need to be supplied for each turbine, and the rotor disk forces are applied to the fluid domain using a set of linear basis functions. Using a linear basis to form the spreading kernel differs from overlapping Gaussians that are typically used for actuator geometries because it forms a partition of unity and allows a continuous representation of the disk surface to be formed with significantly less resolution. This allows us to reduce the resolution required across the rotor disk while still maintaining a uniform disk surface. The reduction in points leads to a subsequent reduction in computational cost and is appropriate for simplified aerodynamic models such as the Joukowski actuator disk. While this model lacks the

structural loading and detailed aerodynamic information available from the OpenFAST coupled ADM turbines, the Joukowski disk model is more computationally efficient. Recent developments regarding this analytic model [19] have also shown that it can capture non-optimal behavior for wind turbines.

Each of the OpenFAST turbine models in the paper was developed from scaled models of publicly available reference turbines, such as the IEA 3.4-130, and no proprietary turbine data was used in the simulations. The scaled models were tuned to match the correct hub-height, rotor size, and power rating, with reasonable approximations of the thrust behavior. The ADM models also underwent a calibration process to accurately match the target power and thrust behavior. The calibration simulations were run in AMR-Wind on a smaller domain with a single turbine, represented using the ADM-Joukowski or ADM-OpenFAST model, placed in the center; three levels of mesh refinement were used to match the primary multi-farm simulations. As shown in Figure 2, the power and thrust predictions from the calibration simulations were compared with the design curves of the respective turbines. Parameters such as the size of the isotropic smoothing kernel and the vortex core size in the Joukowski model were adjusted until the agreement was satisfactory for the wind speeds of interest.

2.5. Case setup and simulation

For the unstable ABL simulation of the AWAKEN wind farm site, a 100 km × 100 km × 2.5 km domain was used which included all five wind farms of interest (see Figure 1). The background mesh resolution (level 0) was 20 m × 20 m × 20 m and was successively refined to achieve 2.5 m × 2.5 m × 2.5 m mesh resolution (level 3) surrounding the turbine rotor regions. For the simulations that included the turbine models, the total mesh size was 21.14B elements, and run on 6000 GPUs on the Summit high-performance computing system at Oak Ridge Leadership Computing Facility, using approximately 1 million GPU-hours to this point.

Table 3. Total farm output averaged over a 10-minute period of the simulation

Farm	Total Output	Cap. Factor	Turbine Type	Avg. Turbine Power
King Plains	166.5 MW	67.1%	GE 2.8-127	1892.5 kW
Armadillo Flats	143.0 MW	57.8%	GE 1.79/1.715-100	1227.7 kW
Breckinridge	72.2 MW	73.6%	GE 1.7-103	1266.8 kW
Chisholm View I & Chisholm View II	159.6 MW	53.2%	GE 1.68-82.5 GE 2.4-107	856.5 kW 1468.7 kW
Thunder Ranch	208.6 MW	70.0%	GE 2.5-116	1754.4 kW
Total	**749.9 MW**	**62.9%**		

The precursor calculation included mesh levels 0, 1, and 2, and was simulated for 15,000 s with a time step of dt=0.25 s to allow the unstable ABL to develop. Afterwards the precursor was simulated for an additional 3,400 s to gather boundary inflow plane data and ABL statistics. After analyzing the precursor profiles, an approximate 900 s window was selected which best matched the unstable ARM conditions in Table 2. This 900 s window allowed for a 5-minute period for the wakes to develop, and an additional 10-minute period to collect wake and turbine statistics. An additional 900-1000 s run after this period is also currently underway to collect additional statistics, with the aim of a total simulation time of close to 30 minutes. The full turbine simulation, using all four mesh levels, was run with a time step of 0.1 s at an approximate CFL of 0.64, and included additional hub-height, rotor plane, and wake sampling planes for postprocessing and analysis. The simulation details and comparison of results will be made available to the public through the Department of Energy's Wind Data Hub located at http://a2e.energy.gov.

3. Results

3.1. Turbine and wind farm power generation

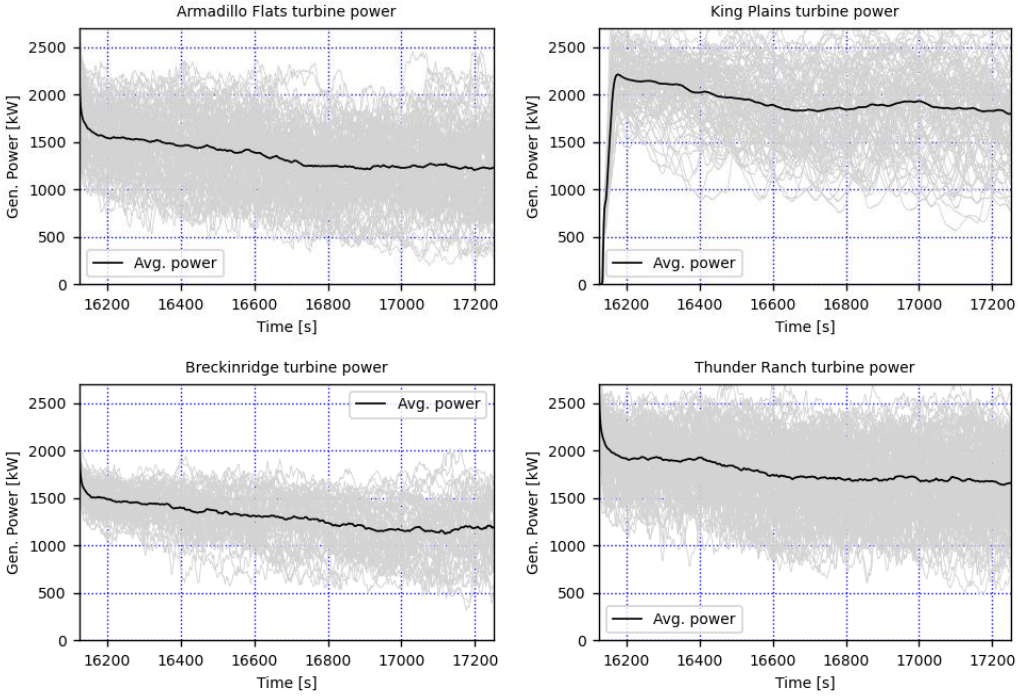

Figure 4 - Instantaneous power production from the Armadillo Flats, King Plains, Breckinridge, and Thunder Ranch wind farms. Each individual turbine power output (grey) and the average turbine power output (black) is plotted.

Details regarding the total power output for each wind farm during the simulation are shown in Table 3 and Figure 4. For the inflow wind speed of 9 m/s, all turbines in the simulation were operating in the variable speed portion of the power curve and rarely reached rated operation during transient gusts. The capacity factor for the five farms in the AWAKEN simulation varied from 53% to 74%, with an overall capacity factor of 63%. As expected, the wind farms that had fewer rows (Breckinridge and Thunder Ranch) experienced fewer wake losses and had higher capacity factors.

3.2. Flow field results

Hub-height contours of the instantaneous and the 10-minute averaged horizontal velocity are shown in Figure 5 for the full AWAKEN domain and King Plains wind farms. In both the instantaneous and the averaged images, we see the dominant presence of large-scale convective structures in the unstable ABL upstream of each farm. The size of these structures was typically in the range of 5-10 km in both the lateral and longitudinal directions, which makes them comparable to the dimensions of the wind farm layouts themselves. These structures alter the local wind speed and direction seen by turbines at different locations within the wind farm, as well as causing deviations in the wake paths on the order of 2-3 degrees over a 10-minute time average. For unstable ABL conditions, the presence of these structures is not surprising; however, they can introduce challenges when attempting to determine the appropriate upstream inflow for determining blockage effects and quantifying wind farm interactions.

To avoid this source of uncertainty, this study uses the precursor simulation, run using the same mesh and boundary conditions without turbines, as a reference solution for comparison. The difference between the time-averaged horizontal velocity in the wind farm simulation and the reference solution without turbines can reveal the effect of upstream wind farms on the inflow of downstream wind farms. For instance, in Figure 6, this difference is shown for the outflow plane of the Breckinridge wind farm and the corresponding inflow plane for Chisholm View. The imprint of the turbine wake deficit is clearly seen on the Breckinridge outflow plane (located approximately 3 km downstream of the farm center); however, the velocity deficit extends past z=400 m. This effect remains visible at inflow plane to Chisholm View, measured approximately 1 km from the upstream turbine row, where the velocity deficit still extends far above the upper rotor tips and decreases the overall shear profile of the incoming ABL.

Similar wake behavior can be seen in the corresponding inflow and outflow planes for the King Plains wind farm (Figure 7). The locations of these vertical planes, shown in Figure 3, are spaced approximately 33.5 D apart and span a distance of 8.5 km both upstream and downstream from the farm center. At the two inflow planes (Plane 1 and 2), the wake velocity deficit from Armadillo Flats is evident on the eastern portion of the plane and extends to elevations of z=250-300 m. The wakes from the King Plains wind turbines themselves, shown in Planes 3 and 4, also expand far above the upper rotor tips and deep into the ABL. This behavior can be explained by the enhanced vertical mixing provided by the unstable conditions and suggests that lidar or radar measurements may be necessary to capture the true extent of wake deficits.

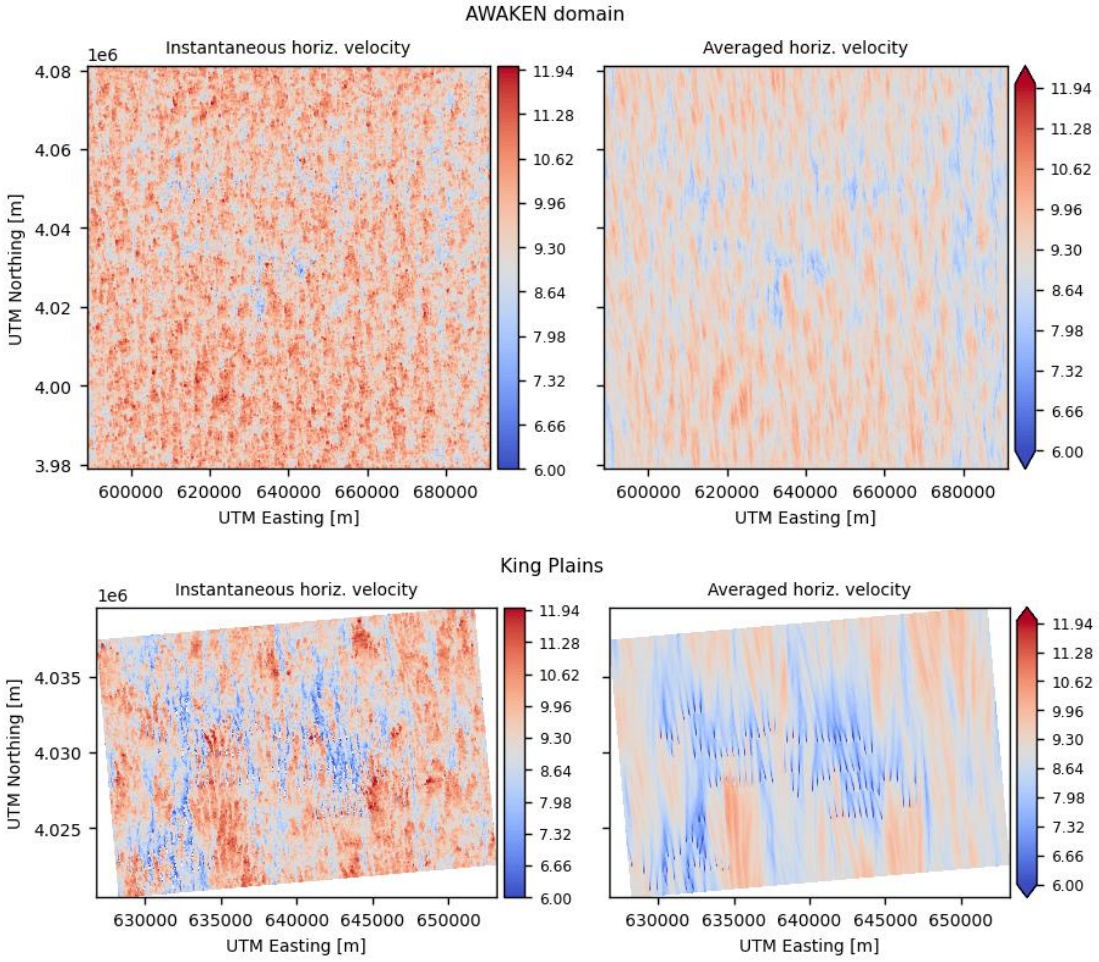

Figure 5 – Instantaneous and time-averaged hub-height horizontal velocity contours (shown in m/s) for the full AWAKEN simulation domain and King Plains wind farms

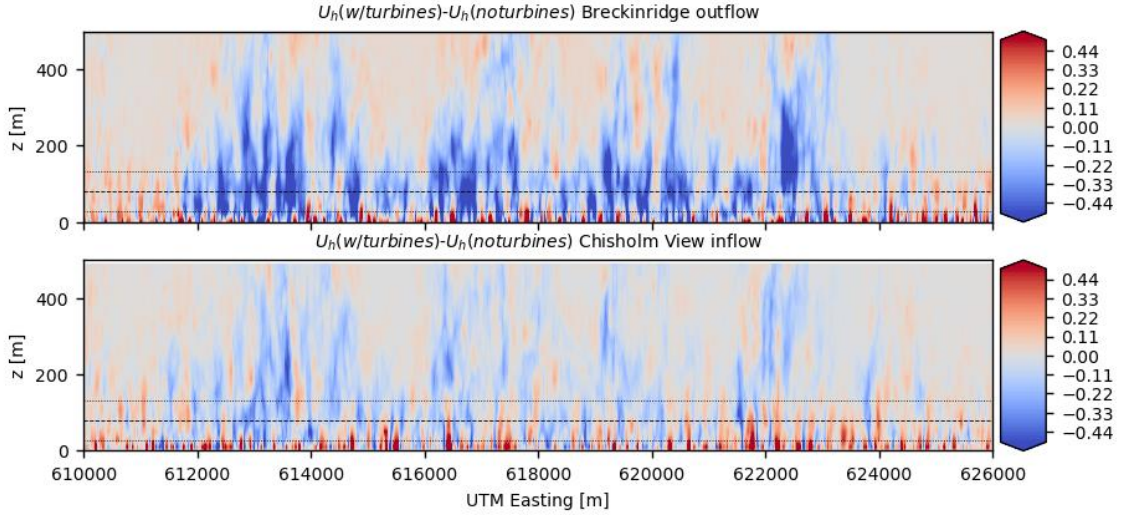

Figure 6 – Outflow plane for Breckinridge (top) and inflow plane for Chisholm View (bottom). The horizontal dashed lines correspond to the hub-height and rotor of the GE 1.7-103 turbines.

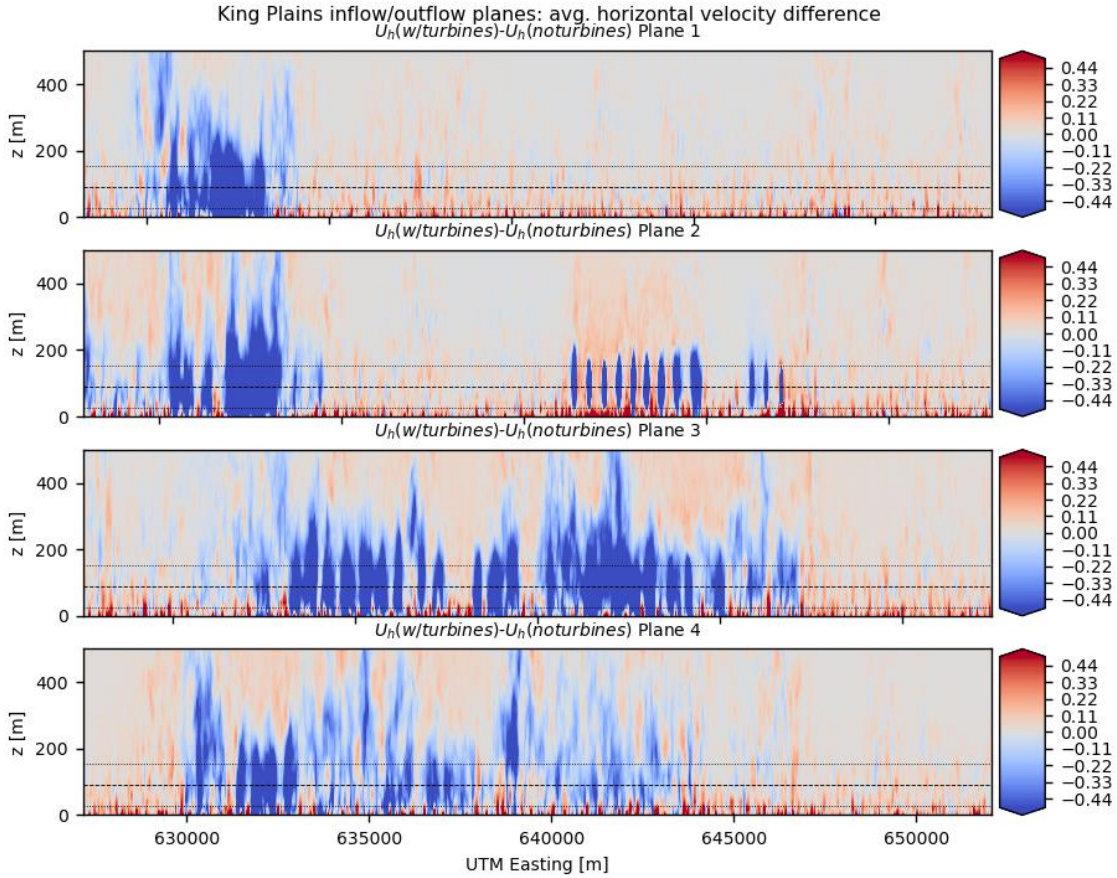

Figure 7 – Inflow/outflow planes for King Plains. The horizontal dashed lines correspond to the hub-height and rotor of the GE 2.8-127 turbines.

The effects of upstream blockage and acceleration can be qualitatively assessed in Figure 8. In this figure the blockage is characterized by the ratio of time averaged velocities

$$U_{h,with\ turbines}/U_{h,no\ turbines}$$

where values smaller than unity indicate blockage slowdown and values larger than unity indicate

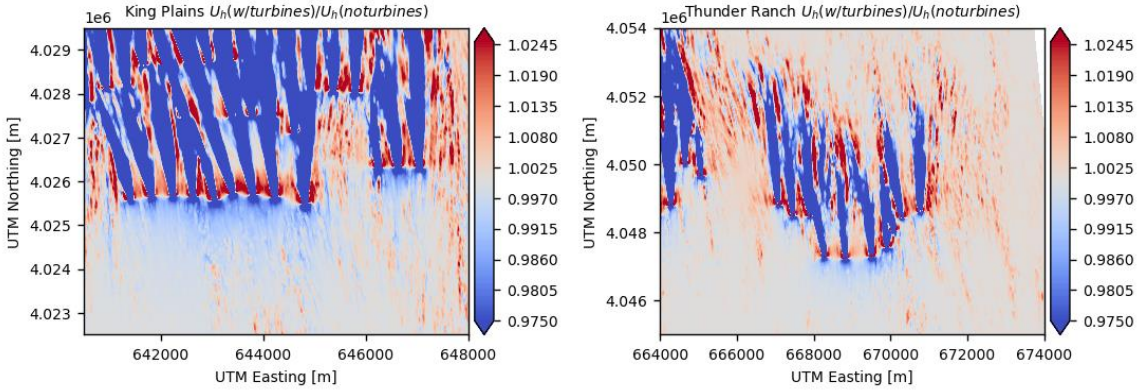

Figure 8 – Blockage contours for the leading wind turbine rows of King Plains (left) and Thunder Ranch (right).

acceleration. At the eastern edges of both King Plains and Thunder Ranch, a noticeable acceleration around the wind farm can be seen. Similar accelerations of approximately 1-2% can be seen between gaps of the wind turbine rows, where channeling of the incoming flow is expected. On the other hand, the incoming flow experiences a noticeable slowdown several diameters upstream of the first row of wind turbines. While this effect is anticipated under stable atmospheric conditions, this slowdown under unstable conditions may be a result of interactions between large scale convective structures and the large number of turbines operating at each wind farm.

Additional insight into the interactions between the large scale convective structures and the wind farms can be found by examining the velocities on the streamwise side planes defined in Figure 3. For instance, the alternating updraft and downdraft motions of the convective structures can be seen in the vertical velocity contours of Figure 9, especially in the precursor simulations without turbines. However, the presence of the wind farm induces additional upward velocity immediately above the operating wind turbines (side plane 2). This additional updraft extends far above the rotor upper tip, and for the King Plains wind farm, a positive vertical velocity difference be seen above z=400m.

The induced vertical velocity above the turbines also magnifies the obstruction presented to the incoming flow, as seen in the contours of the normalized horizontal velocity in Figure 10. The slowdown ahead of the first-row turbines extends far above the rotor upper tip, and a distinct jump between the upstream slowdown and downstream acceleration can also be seen above each turbine location. A noticeable slowdown is visible far upstream of the turbine location, on the order of 1% wind speed reduction several kilometers ahead of the first row. This behavior is consistent with the deceleration of a large-scale coherent structure to an upstream obstruction of approximately similar size. In future work, we will compare the blockage patterns from this unstable ABL with the corresponding blockage behavior under stable stratification.

4. Summary and conclusions

In this work, the full domain of five wind farms was simulated as a part of the AWAKEN field campaign. Using the AMR-Wind LES code, 541 wind turbines were simulated in a 100 km×100 km domain under unstable ABL conditions matching measured atmospheric data. The results qualitatively illustrated the interactions between wind farms and large scale ABL structures in the flow, as well as the extent of downstream wake penetration in the flow and blockage effects around wind farms. Future work will also include verifying the observed vertical structures through additional targeted simulations along with validation through data from the AWAKEN field experiment. Additional postprocessing of the simulations in future work will also help determine what phenomena are possible to measure in planned lidar and radar data sets that will allow for comparison

with different wind farm prediction tools. Planned future simulations under stable atmospheric conditions will augment the current results to be contrasted with different stratifications.

Acknowledgements

This research was supported by the Wind Energy Technologies Office of the U.S. Department of Energy (DOE) Office of Energy Efficiency and Renewable Energy. Sandia National Laboratories is a multimission laboratory managed and operated by National Technology & Engineering Solutions of Sandia, LLC, a wholly owned subsidiary of Honeywell International Inc., for the U.S. DOE's National Nuclear Security Administration under contract DE-NA0003525. The views expressed in the article do not necessarily represent the views of the U.S. DOE or the United States Government.

This research was supported by the Exascale Computing Project (17-SC-20-SC), a joint project of the U. S. Department of Energy Office of Science and the National Nuclear Security Administration, responsible for delivering a capable exascale system, including software, applications, and hardware technology, to support the nation's exascale computing imperative. This research also used resources of the Oak Ridge Leadership Computing Facility, which is a DOE Office of Science User Facility supported under Contract DE-AC05-00OR22725, which was provided through the ASCR Leadership Computing Challenge (ALCC) program.

This work was authored in part by the National Renewable Energy Laboratory, operated by Alliance for Sustainable Energy, LLC, for the U.S. Department of Energy (DOE) under Contract No. DE-AC36-08GO28308. Funding provided by U.S. Department of Energy Office of Energy Efficiency and Renewable Energy Wind Energy Technologies Office. The views expressed in the article do not necessarily represent the views of the DOE or the U.S. Government. The U.S. Government retains and the publisher, by accepting the article for publication, acknowledges that the U.S. Government retains a nonexclusive, paid-up, irrevocable, worldwide license to publish or reproduce the published form of this work, or allow others to do so, for U.S. Government purposes.

This article has been authored by an employee of National Technology & Engineering Solutions of Sandia, LLC under Contract No. DE-NA0003525 with the U.S. Department of Energy (DOE). The employee owns all right, title and interest in and to the article and is solely responsible for its contents. The United States Government retains and the publisher, by accepting the article for publication, acknowledges that the United States Government retains a non-exclusive, paid-up, irrevocable, world-wide license to publish or reproduce the published form of this article or allow others to do so, for United States Government purposes. The DOE will provide public access to these results of federally sponsored research in accordance with the DOE Public Access Plan https://www.energy.gov/downloads/doe-public-access-plan. SAND 2023-03166C

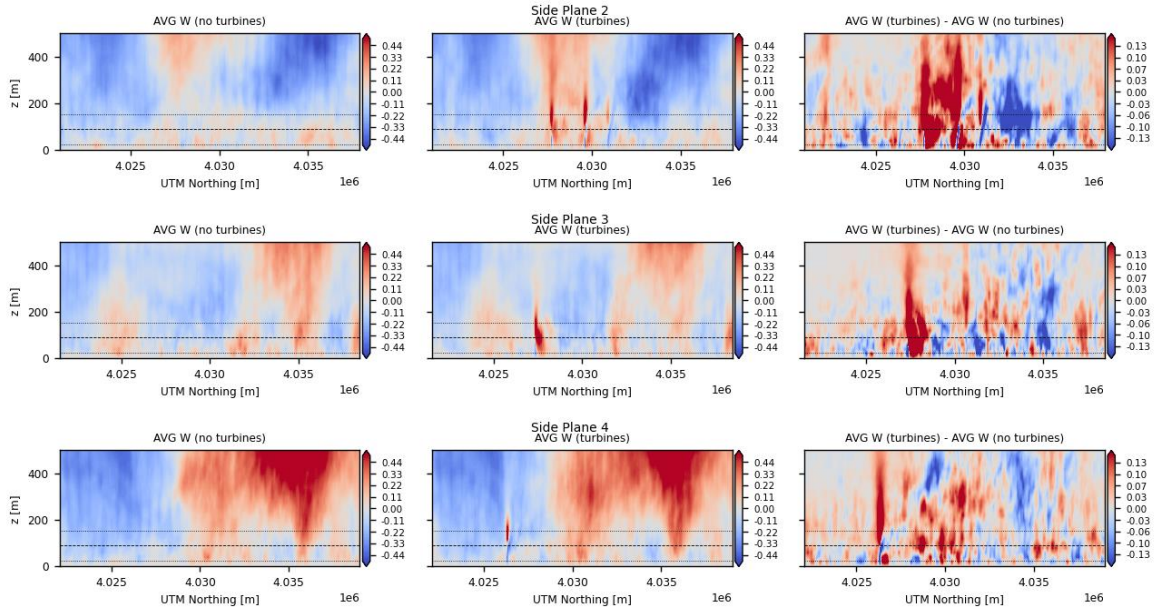

Figure 9 – Vertical velocity contours on the side planes of King Plains wind farm.

References

[1] D. Mehta, A. H. van Zuijlen, B. Koren, J. G. Holierhoek and H. Bijl, "Large Eddy Simulation of Wind Farm Aerodynamics: A Review," *Journal of Wind Engineering and Industrial Aerodynamics,* vol. 133, pp. 1-17, 2014.

[2] S. P. Breton, J. Sumner, J. N. Sorensen, K. S. Hansen, S. Sarmast and S. Ivanell, "A Survey of Modelling Methods for High-Fidelity Wind farm Simulations Using Large Eddy Simulation," *Philos Trans A Math Phys Eng Sci,* no. 2091, 2017.

[3] G. Centurelli, L. Vollmer, J. Schmidt, M. Dorenkamper, M. Schroder, L. J. Lukassen and J. Peinke, "Evaluating Global Blockage Engineering Parametrizations with LES," *Journal of Physics Conference Series,* vol. Wakes Conference 2021, no. 1934, 2021.

[4] A. Kirby, T. Nishino and T. D. Dunstan, "Two-Scale Interaction of Wake and Blockage Effects in Large Wind Farms," *Journal of Fluid Mechanics,* vol. 953, no. A39, 2022.

[5] M. Sanchez Gomez, J. K. Lundquist, J. D. Mirocha, R. S. Arthur, D. Muñoz-Esparza and R. Robey, "Can Lidars Assess Wind Plant Blockage in Simple Terrain? A WRF-LES Study," *Journal of Renewable and Sustainable Energy,* vol. 14, no. 6, 2022.

[6] J. M. I. Strickland, S. N. Gadde and R. J. A. M. Stevens, "Wind Farm Blockage in a Stable Atmospheric Boundary Layer," *Renewable Energy,* vol. 197, pp. 50-58, 2022.

[7] J. M. I. Strickland and R. J. A. M. Stevens, "Investigating Wind Farm Blockage in a Neutral Boundary Layer Using Large-Eddy Simulations," *European Journal of Mechanics - B/Fluids,* vol. 95, pp. 303-314, 2022.

[8] J. Bleeg, M. Purcell, R. Ruisi and E. Traiger, "Wind Farm Blockage and the Consequences of Neglecting Its Impact on Energy Production," *Energies,* vol. 11, no. 6, 2018.

[9] J. Schneemann, F. Theuer, A. Rott, M. Dörenkämper and M. Kühn, "Offshore wind farm global blockage measured with scanning lidar," *Wind Energy Science,* vol. 6, no. 2, pp. 521-538, 2021.

[10] A. Platis, S. K. Siedersleben, J. Bange, A. Lampert, K. Barfuss, R. Hankers, B. Canadillas, R. Foreman, J. Schulz-Stellenfleth, B. Djath, T. Neumann and S. Emeis, "First In Situ Evidence of Wakes in the Far Field Behind Offshore Wind Farms," *Scientific Reports,* vol. 8, no. 2163, 2018.

[11] B. Cañadillas, R. Foreman, V. Barth, S. Siedersleben, A. Lampert, A. Platis, B. Djath, J. Schulz-Stellenfleth, J. Bange and T. Neumann, "Offshore Wind Farm Wake Recovery: Airborne Measurements and its Representation in Engineering Models," *Wind Energy,* vol. 23, no. 5, pp. 1249-1265, 2020.

[12] A. Sebastiani, F. Castellani, G. Crasto and A. Segalini, "Data Analysis and Simulation of the Lillgrund Wind Farm," *Wind Energy,* vol. 24, no. 6, pp. 634-648, 2020.

[13] P. Moriarty, N. Bodini, L. Cheung, N. Hamilton, T. Herges, C. Kaul, S. Letizia, M. Pekour and E. Simley, "Overview of recent observations and simulations from the American Wake Experiment (AWAKEN) field campaign," in *IOP Conference Series - Wake Conference 2023 (submitted)*, Visby, Sweden, 2023.

[14] M. Sprague, S. Ananthan, G. Vijayakumar and a. M. Robinson, "ExaWind: A multi-fidelity modeling and simulation environment for wind energy," in *Journal of Physics Conference Series*, 2020.

[15] A. S. Almgren, J. B. Bell, P. Colella, L. H. Howell and M. L. Welcome, "A conservative adaptive projection method for the variable density incompressible Navier--Stokes equations," *Journal of Computational Physics,* vol. 142, no. 1, pp. 1-46, 1998.

[16] K. Sverdrup, N. Nikiforakis and A. Almgren, "Highly parallelisable simulations of time-dependent viscoplastic fluid flow with structured adaptive mesh refinement," *Physics of Fluids,* vol. 30, no. 9, p. 093102, 2018.

[17] C.-H. Moeng, "A large-eddy-simulation model for the study of planetary boundary-layer turbulence," *Journal of the Atmospheric Sciences,* vol. 41, no. 13, pp. 2052-2062, 1984.

[18] J. N. Sørensen, K. Nilsson, S. Ivanell, Henrik Asmuth and R. F. Mikkelsen, "Analytical body forces in numerical actuator disc model of wind turbines," *Renewable Energy,* vol. 147, pp. 2259-2271, 2020.

[19] J. Sorensen, "Generalized analytical body force model for actuator disc computations of wind turbines," *Wind Energy Science Discussions,* vol. 2022, pp. 1-19, 2022.

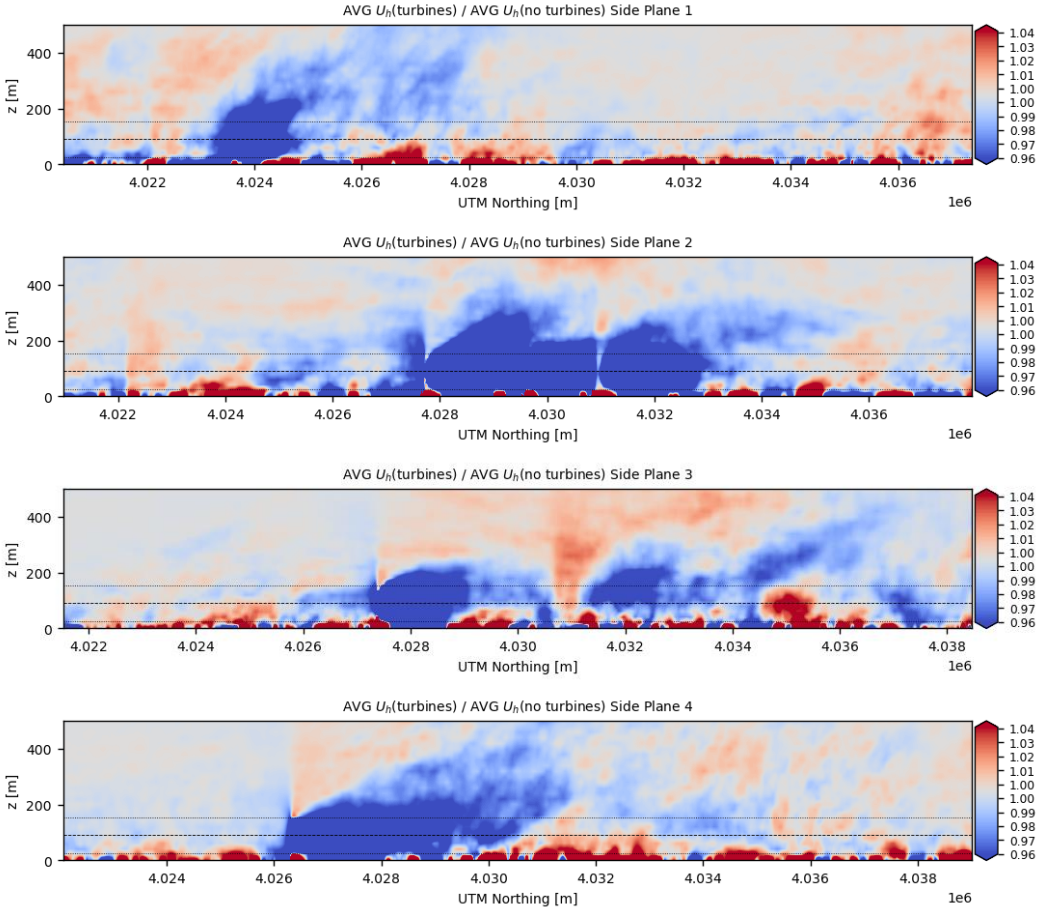

Figure 10 – Normalized horizontal velocity contours on the side planes of King Plains wind farm.